

# Isotropic-to-nematic nucleation in suspensions of colloidal rods

Alejandro Cuetos,<sup>\*a</sup> René van Roij<sup>b</sup> and Marjolein Dijkstra<sup>a</sup>

Received 12th October 2007, Accepted 21st December 2007

First published as an Advance Article on the web 31st January 2008

DOI: 10.1039/b715764a

Using computer simulations, we study the isotropic-to-nematic nucleation in a fluid of colloidal hard rods as well as in a mixture of colloidal rods and non-adsorbing polymer. In order to follow the transformation of the system from the isotropic to the nematic phase, we use a new cluster criterion that enables us to distinguish the nematic clusters from the isotropic fluid phase. Applying this criterion in Monte Carlo simulations, we find two different regimes depending on the supersaturation. At low supersaturation we find nucleation and growth, while at higher supersaturation spinodal decomposition is observed. We determine the height of the nucleation barrier, and we study the structure as well as the shape of the nematic clusters. We discuss our simulation results in the light of classical nucleation theory.

## I. Introduction

Nucleation is the process whereby a thermodynamically metastable state evolves into a stable one, *e.g.* the freezing of undercooled water into ice, the condensation of a supersaturated vapor into a liquid, or the formation of gaseous bubbles in an superheated liquid phase. The framework with which phenomena like these have been described traditionally is classical nucleation theory (CNT), which is based on the notion that a thermal fluctuation spontaneously generates a small spherical “droplet” of the thermodynamically stable phase into the bulk of the metastable phase.<sup>1</sup> This droplet is assumed to be separated from the metastable bulk by a sharp step-like interface. The tension of this interface gives rise to a tendency to shrink the size of the droplet, and hence small droplets (with their large surface-to-volume ratio) have a large probability to dissolve. Only if the droplet exceeds a critical size, CNT predicts a crossing of the free-energy barrier and the droplet can grow to form the new stable bulk phase. In recent years, many new simulation techniques have been developed to study nucleation, such as umbrella-sampling,<sup>2–4</sup> transition-path-sampling<sup>5–7</sup> or forward-flux-sampling methods.<sup>8–10</sup> Substantial progress in our understanding of gas–liquid and fluid–solid nucleation of spherical particles is due to these computer simulations,<sup>11–13</sup> but also due to density functional theory calculations.<sup>14–17</sup> For instance, recent studies have shown that the structure of the critical nucleus at its center may be completely different from the bulk phase to be formed, and that its interface with the surrounding metastable state may have a non-trivial density and structural profile that is not at all sharp and step-like.<sup>11,12,14–17</sup> Moreover, very recent simulation work indicates that thermal fluctuations allow for a whole ensemble of transition states instead of a single critical nucleus.<sup>5</sup>

Nucleation is even more complicated, and interesting, in the case of non-spherical particles. Due to the anisotropy of the

particles, these systems can also form liquid-crystalline phases, which enriches the phase behaviour considerably. Recent experiments with supersaturated suspensions of colloidal rods and non-adsorbing polymer show a fascinating rich phenomenology with novel and complex metastable structures like spindle-shaped nematic droplets (“tactoids”), surface-induced smectic phases on the surface of metastable nematic droplets, individual smectic membranes winding off from tactoids as twisted ribbons, *etc.*<sup>18</sup> Another topic that has received a lot of interest is the existence or non-existence of isotropic-to-nematic (I–N) spinodal decomposition in suspensions of rod-like particles. The existence of spinodal decomposition was previously predicted by Onsager for suspensions of hard rods with infinite aspect ratios.<sup>37</sup> Using small-angle light scattering Van Bruggen *et al.* found indeed two different regimes in the I–N transformation in a fluid of colloidal rods, depending on the supersaturation.<sup>19</sup> These authors characterized the transformation in the more dilute systems as nucleation and growth, while spinodal decomposition was observed in the more concentrated systems. Similar results have been found recently in solutions of F-actin,<sup>20</sup> or in dispersions of rod-like viruses under shear conditions.<sup>21,22</sup> We note, however, that in Ref. 21 and 22 the nucleation and growth phenomena are found at high concentration while the spinodal decomposition is found at low density. The reason for this is that the initial state is a shear-induced nematic phase. Recent experimental work on the structure of the clusters shows the formation of ellipsoidal nematic tactoids with the rods oriented in the direction of the long axis of the droplets.<sup>20,23,24</sup>

In contrast with experimental work, simulation studies on the nucleation of anisotropic particles are more scarce and less conclusive. The isotropic-to-solid transition has been explored in systems of short hard rods by Schilling and Frenkel<sup>25,26</sup> These authors show that the growth of the crystal starts with the formation of a single crystalline layer with hexagonal order. Subsequently, the growth of the crystal is hampered by rods that align parallel to the top and bottom surface of the crystallite, yielding self-poisoning of the crystal nucleus. In addition, they calculated the free energy as a function of cluster size, and found that the system never crosses a nucleation barrier beyond which the

<sup>a</sup>Soft Condensed Matter, Debye Institute for NanoMaterials Science, Utrecht University, Princetonplein 5, Utrecht, 3584 CC, The Netherlands. E-mail: a.cuetos@phys.uu.nl

<sup>b</sup>Institute for Theoretical Physics, Utrecht University, Leuvenlaan 4, Utrecht, 3584 CE, The Netherlands

crystallites would grow spontaneously. In Ref. 27, the isotropic–nematic spinodal is investigated using Brownian dynamics simulations in fluids of hard rods for various elongations.

In the present paper, we study the I–N transition in a fluid of hard spherocylinders (HSC fluid) for two elongations. We find, in agreement with experimental studies, two different regimes depending on the supersaturation. At low supersaturation, we observe nucleation and growth, while at high supersaturation, spinodal decomposition is observed. We also find, in the nucleation and growth regime, the formation of ellipsoidal nematic clusters. We compare our simulation results with the predictions of classical nucleation theory. A brief account of a part of this work has already been published elsewhere.<sup>28</sup> Moreover, we study the I–N transformation in a system of colloidal hard rods and non-absorbing polymers using an effective polymer-mediated pair potential for the colloidal rods.<sup>29</sup>

This paper is organized as follows. In Section II, we describe the model and the simulation techniques that we use. In Section III, we discuss classical nucleation theory and we extend this theory to nonspherical particles, *i.e.*, we introduce an anisotropic surface tension and we consider aspherical droplets. In Section IV, we present the results, and we end with some concluding remarks in Section V.

## II. Model and simulation method

### A. Models

We first consider a suspension of colloidal rods, modelled by hard spherocylinders (HSC) with diameter  $\sigma$  and length  $L$ . This model has been studied extensively, and its equilibrium bulk phase diagram is well known.<sup>30,31</sup> We perform Monte Carlo simulations of colloidal hard rods with elongations  $L^* = L/\sigma = 5$  and  $L^* = 15$ . These systems show a phase transition from an isotropic fluid phase to an orientationally ordered nematic phase. For elongation  $L^* = 5$  the transition occurs at pressure  $P_{IN}^* = 1.117$ , where we define  $P^* = \beta P \sigma^3$ ,  $\beta = 1/k_B T$ ,  $k_B$  is Boltzmann's constant, and  $T$  the temperature, and at  $P_{IN}^* = 0.097$  for  $L^* = 15$ .<sup>31</sup> For  $L^* = 5$ , the transition is weakly first order without a clear density jump.<sup>31</sup> For  $L^* = 15$  the I–N transition is of first order with a density jump of about 20%.

In addition, we consider a mixture of colloidal hard rods with non-adsorbing polymers. Our interest in this mixture is triggered by recent experiments on mixtures of rod-like viruses and non-adsorbing polymers, which show novel and intriguing nucleation paths, including many new metastable structures.<sup>18</sup> To study this system we use the effective polymer-mediated pair potential proposed recently for the rods.<sup>29</sup> We refer the reader to Ref. 29 for more details on the derivation of this effective pair potential. Here we only give a brief account.

We map this binary mixture of hard rods with non-adsorbing polymer onto an effective one-component system by integrating out the degrees of freedom of the polymer in the partition function. We employ the effective pair potential approximation to the effective Hamiltonian. The effective pair potential of two rods reads

$$\Phi(\mathbf{R}_{ij}; \hat{\omega}_i, \hat{\omega}_j) = \Phi_{rr}(\mathbf{R}_{ij}; \hat{\omega}_i, \hat{\omega}_j) + \Phi_{dep}(\mathbf{R}_{ij}; \hat{\omega}_i, \hat{\omega}_j) \quad (1)$$

where  $\mathbf{R}_{ij} = \mathbf{R}_i - \mathbf{R}_j$  with  $\mathbf{R}_i$  the center-of-mass of spherocylinders  $i$ , and where  $\hat{\omega}_i$  denotes the orientation of rod  $i$ . The bare

rod–rod pair interaction  $\Phi_{rr}$  is modelled here as a hard interaction, *i.e.*,  $\beta\Phi_{rr} = \infty$  if two particles overlap and 0 otherwise, while  $\Phi_{dep}$  is a pairwise additive depletion potential. An explicit expression for  $\Phi_{dep}$  can be found in Ref. 29. Hence, the effective pair potential (1) consists of a repulsive part and an attractive part, that both depend on the relative orientations of the two particles,  $\hat{\omega}_i$  and  $\hat{\omega}_j$ , and on the center-of-mass distance vector  $\mathbf{R}_{ij}$ . The attractive interaction between two rods is stronger for parallel rods than for perpendicular rods.<sup>29</sup>

Phase diagrams of colloidal rods with  $L^* = 5$ , interacting with such potentials, have been determined using computer simulations. They display a stable isotropic, nematic, smectic, and crystalline phase, depending on the rod-packing fraction and polymer fugacity. Due to the attraction between the rods, the I–N transition is stronger first order than that in a fluid of pure hard rods with the same elongation. Below we study nucleation for  $L^* = 5$ , a polymer fugacity  $z_p = 0.514$  (corresponding to a maximum attraction of about  $1k_B T$  for parallel rods), and a radius of gyration of the polymer  $R_g = 0.25\sigma$ . The I–N transition is at a pressure  $P_{IN}^* = 0.86$ , and the density difference between the two coexisting phases is about 5%.

### B. Simulation Details

In order to follow the transition from the isotropic to the nematic phase, we perform standard Monte Carlo simulations in the isobaric–isothermal ensemble (MC-NPT), *i.e.*, we fix the number of particles  $N$ , the temperature  $T$ , and the pressure  $P^*$  at values higher than that at I–N bulk coexistence. To this end, we compress a well-equilibrated configuration of the coexisting bulk isotropic phase to the desired supersaturated pressure. Subsequently, we perform successive simulations, monitoring different order parameters that provide information about the intermediate situations in the I–N transformation. In all our simulations, we employ a rectangular simulation box with periodic boundary conditions. Depending on the model and on the elongation of the particles, different particle numbers have been employed. We present simulations with  $N = 8649$ , 4320, and 2160 particles. More details are presented when we discuss the results. In all our simulations, the acceptance ratio is kept within 30–40% for the orientational and translational moves of the particles, and within 20–30% for the attempts to change the volume. Box volume changes are attempted by randomly changing the length of one of the sides of the simulation box, with the restriction that the box length remains larger than twice the length of the rods in order to avoid multiple overlaps.

At low supersaturation, *i.e.*, at pressures slightly higher than the coexistence pressure, the free-energy barrier to nucleation is very high. Hence, spontaneous fluctuations that would bring the system to the top of the free-energy barrier, which are needed for a spontaneous subsequent growth of the stable phase, is very unlikely. In other words, nucleation is a rare event, or an activated process for which the waiting time for it to occur is much longer than the event itself. Events of such a nature are intrinsically difficult to study with conventional simulation methods, as most of the CPU time would be wasted on the long waiting times between the nucleation events. It is therefore virtually impossible to observe in a standard MC-NPT simulation the growth of a nematic cluster beyond its critical size and hence the

spontaneous transition to the nematic phase. Standard MC-NPT simulations are therefore only used to study spinodal decomposition and nucleation and growth at high supersaturations, *i.e.*, at state points that lie close to the spinodal curve or beyond.

In order to study rare events such as nucleation, many simulation techniques have been developed, *e.g.*, transition-path-sampling techniques<sup>5,6,7</sup> or forward-flux-sampling methods.<sup>8,9,10</sup> In this paper, we use umbrella sampling to study the I–N nucleation.<sup>2,3,4</sup> Umbrella-sampling methods have been employed to compute the free-energy nucleation barrier within the Bennett–Chandler approach and have been used to study the gas–liquid<sup>32,33,34</sup> and fluid–solid<sup>9,11,12,35</sup> nucleation in fluids of spherical particles.

This method allows us to bias the sampling to configurations that contain clusters with a certain size. We use the number of particles, say  $n$ , in the largest nematic cluster, as an order parameter. Following Ref. 32, we use a biasing potential  $W$ , which is a harmonic function of the cluster size  $n$ :

$$\beta W(n(\mathbf{r}^N, \hat{\omega}^N)) = \frac{1}{2} \kappa_n [n(\mathbf{r}^N, \hat{\omega}^N) - n_0]^2, \quad (2)$$

where  $\mathbf{r}^N$  and  $\hat{\omega}^N$  are the positions and orientations of all  $N$  particles in the simulation. The result of this biasing potential is that a certain window of values of the order parameter will be sampled. The constants  $\kappa_n$  and  $n_0$  determine the width and the location of the window. By increasing the value of  $n_0$ , we can increase the size of the largest nematic cluster in our system, which enables us to cross the nucleation barrier. In our simulations, the values for  $\kappa_n$  lie in the range 0.1–0.15. As the computation of the size of the largest cluster is very time consuming, we only apply the biasing potential after trajectories of ten MC cycles without biasing potential, and we then accept this trajectory with a statistical weight that does include the biasing potential. If we define the average number of clusters with  $n$  particles by  $\langle N_n \rangle$ , one can calculate the probability distribution  $P(n) = \langle N_n \rangle / N$ . We perform simulations with varying values for  $n_0$  spanning all values of  $n$  between the metastable isotropic and the stable nematic phase. We can then determine the Gibbs free-energy barrier for the formation of a nematic cluster of size  $n$  by:

$$\Delta G(n) = -k_B T \ln P(n). \quad (3)$$

The cluster at the top of the nucleation barrier, where  $\Delta G(n)$  is at a maximum, is defined as the critical cluster. A cluster that exceeds the critical size (a postcritical cluster), will spontaneously grow and will form the stable nematic phase in order to minimize the free energy, while most subcritical clusters will redissolve spontaneously. Umbrella-sampling techniques allow us to calculate the nucleation barrier, but also to stabilize critical, subcritical and postcritical cluster in order to study the internal structure and the shape of these clusters.

For the calculation of the nucleation barrier, using umbrella sampling, we need a criterion that can identify the nematic clusters from the isotropic fluid phase. For the case of spherical particles several cluster criteria have been defined to study gas–liquid<sup>32</sup> and fluid–solid<sup>12</sup> transitions. For fluids of elongated particles, Schilling and Frenkel<sup>25,26</sup> have defined a cluster criterion in order to study the isotropic–solid transition in a fluid of hard spherocylinders with elongation  $L^* = 2$ . This criterion

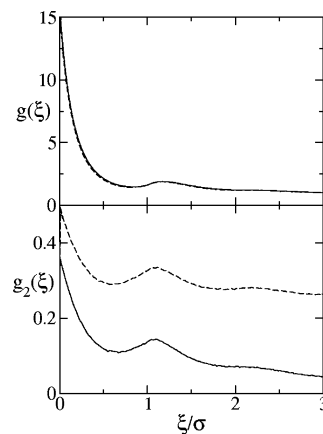


**Fig. 1** Radial distribution function  $g(\xi)$  (top panel) and orientational pair correlation function  $g_2(\xi)$  (bottom panel) as a function of the surface–surface distance  $\xi$  for an isotropic (solid line) and a nematic (dashed line) phase near coexistence in a HSC fluid with  $L^* = 5$ .

assumes that two particles belong to the same cluster if the surface-to-surface distance between the two particles is smaller than  $0.5\sigma$  and the absolute value of the dot product of the two unit vectors that define the orientations of the rods are larger than 0.995. Using this cluster criterion for fluids of sufficiently long, hard spherocylinders, which exhibit a stable nematic phase, we were not able to distinguish the nematic phase from the isotropic phase. We therefore developed a new cluster criterion.<sup>28</sup>

To this end, we study in more detail the structure of the coexisting isotropic and nematic phase of a HSC fluid with  $L^* = 5$ . Fig. 1 shows that the radial distribution functions of the coexisting isotropic and nematic phase are very similar, while the orientational pair correlation functions differ considerably. To be more specific, we find long-range orientational order in the nematic phase, while there is only short-range orientational order in the isotropic phase (for details on the calculation see Ref. 30). The short-range orientational order that is present in both the isotropic and nematic phase might be the reason that the cluster criterion in Ref. 25 and 26 cannot be used to distinguish nematic clusters from the isotropic phase, as it only considers neighboring particle pairs. In our cluster criterion, we exploit the difference in orientational order at larger distances for the isotropic and nematic phase. We first make a distinction between particles that have a nematic-like and an isotropic-like environment. Particle  $i$  is nematic-like if its local environment has an orientational order significantly larger than in the isotropic phase. The local environment of particle  $i$  is defined by all particles  $j$  with a surface-to-surface distance  $\xi_{ij} \leq 1.5\sigma$ , *i.e.*, such that it is not only defined by the nearest neighbors, but also by the next-nearest neighbors, thereby taking advantage of the long-ranged orientational order in the nematic phase. The local orientational order of particle  $i$  is defined by:

$$S(i) = \frac{1}{n_i} \sum_{j=1}^{n_i} \left( \frac{3}{2} |\hat{\omega}_j \cdot \hat{\omega}_i|^2 - \frac{1}{2} \right), \quad (4)$$

where  $\hat{\omega}_j$  is the unit orientation vector of particle  $j$  and  $n_i$  the number of particles with  $\xi_{ij} \leq 1.5\sigma$ . We have adopted the cluster criterion so that particle  $i$  is nematic-like if  $S(i) > K_1$ , where  $K_1$  is

a threshold value that has to be optimized for each model. After identifying the nematic particles in the system, we determine the nematic cluster with the criterion that two particles  $i$  and  $j$  belong to the same cluster if  $\xi_{ij} < 0.5\sigma$  and  $|\hat{\omega}_i \cdot \hat{\omega}_j| > K_2$ , with  $K_2$  another adjustable threshold value. We have optimized the threshold values  $K_1$  and  $K_2$  using the criterion i) that for a nematic bulk phase, a considerable fraction of the particles, say  $> 90\%$ , belongs to the nematic cluster, and ii) that for an isotropic bulk phase, a tiny fraction of the particles,  $< 2\%$  belongs to nematic clusters. We have performed several trial runs to optimize the threshold values and we have chosen  $K_1 = 0.4$  and  $K_2 = 0.85$  for the HSC system, and  $K_1 = 0.6$  and  $K_2 = 0.85$  for the rod-polymer mixture.

We perform MC-NPT simulation of a HSC fluid with  $L^* = 15$  at several state points in the isotropic and nematic phase in a simulation box with 4320 particles. In Fig. 2, we show the cluster size distribution  $\langle N_n \rangle$  determined by our cluster criterion for a low-density isotropic state, a high-density nematic state, and for an isotropic and nematic phase at bulk coexistence. Fig. 2 shows that there is a clear distinction in the cluster size distributions of the isotropic and nematic phase. In the isotropic states, we only find clusters with particle numbers  $n < 20$ . In the nematic states, we observe clusters that are considerably larger in size, while only a few smaller clusters, *i.e.*,  $n < 10$ , are observed. Hence, our cluster criterion enables us to distinguish the nematic from the isotropic phase. We wish to make two remarks here. First, we note that not all particles belong to a nematic cluster in the nematic phase. This is because the orientational distribution function is not a Delta function, but resembles more a Gaussian distribution with a non-zero probability to find particles with orientations deviating somewhat from the nematic director.<sup>36,37,38</sup> Secondly, we also find that the size of the nematic cluster increases upon increasing the pressure, which is consistent with the increase in nematic order upon increasing the density.

To analyze our simulation results, we employ order parameters that are frequently used in liquid-crystal studies. For example, we calculate the nematic order parameter  $S$  of the whole system as well as of the nematic clusters. This nematic order parameter is defined by the largest eigen value of the standard  $3 \times 3$  nematic order parameter tensor. The corresponding eigen vector defines the nematic director  $\mathbf{n}$ , which denotes the

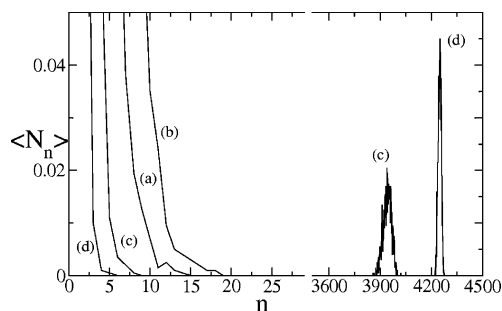


**Fig. 2** Distribution of the number of particles  $n$  in the nematic clusters in a HSC fluid with  $L^* = 15$  for (a) a low-density isotropic state,  $P^* = 0.075$ , (b) an isotropic state at bulk coexistence,  $P^* = 0.097$ , (c) a nematic state at bulk coexistence, and (d) a high-density nematic state,  $P^* = 0.12$ . Note the discontinuity in the horizontal axis. The total number of particles is 4320.

preferred orientation of the particles. To study the structure of the nematic clusters we calculate the density profile  $\rho^*(z, r)$  as a function of the distance from the center-of-mass of the cluster in the direction parallel ( $z$ ) and perpendicular ( $r$ ) to the nematic director of the cluster. We again make a distinction between particles that have an isotropic-like and a nematic-like environment using the same criterion as defined before. We calculate these density profiles for i) all particles that belong to the nematic cluster according to our cluster criterion, ii) for all isotropic-like (non-nematic-like) particles (particles with an isotropic-like environment), and iii) for all isotropic-like and nematic-like particles regardless of their environment. We also calculate the nematic order parameter profiles  $S(z, r)$  of all particles (nematic and isotropic) in the system (not only in the nematic cluster). The nematic order parameter profile is defined by  $S(z, r) = \langle 3|\hat{\omega}(z, r) \cdot \mathbf{n}|^2 - 1 \rangle / 2$ , where  $\mathbf{n}$  is the nematic director of the cluster.

### III. Theory

We check the validity of CNT for liquid-crystalline transitions by comparing its predictions with our simulation results. We focus our attention on the I-N nucleation in a HSC fluid. Within standard CNT for spherical droplets,<sup>1</sup> the Gibbs free-energy barrier that separates the metastable parent phase from the stable final phase is written as  $\Delta G = \gamma A - |\Delta\mu|\rho V$ , where  $\gamma$  is the surface tension of the planar interface between the two coexisting phases,  $A = 4\pi R^2$  is the surface area of the spherical nucleus (radius  $R$ ) of the new phase at density  $\rho$ ,  $\Delta\mu < 0$  is the chemical potential difference between the phase inside the nucleus and that of the supersaturated bulk phase, and  $V = (4\pi/3)R^3$  is the volume of the nucleus. For a given  $\Delta\mu$  and  $\rho$ , the radius  $R_{\text{crit}} = 2\gamma/\rho|\Delta\mu|$  of the critical nucleus follows from  $\partial\Delta G/\partial R|_{R_{\text{crit}}} = 0$ , and the resulting nucleation barrier reads  $\Delta G_{\text{crit}} = (16\pi/3)\gamma^3/(\rho|\Delta\mu|^2)$ .

For non-spherical particles such as rods, these expressions need to be modified because i) the surface tension depends on the relative angle of the interface normal  $\mathbf{q}$  and the nematic director  $\mathbf{n}$  of the nematic phase, ii) the critical nucleus is not expected to be a sphere, and iii) the free energy of a nematic nucleus should include an elastic energy cost for a possible deformation of the director field. Here we assume that the anisotropy of the surface tension can be characterized by a single anisotropy parameter  $\omega$  such that the tension reads  $\gamma(1 + \omega(\mathbf{q} \cdot \mathbf{n})^2)$ , where  $\gamma$  is the tension for the planar geometry  $\mathbf{q} \perp \mathbf{n}$ . We also assume planar anchoring of the director field to the interface, *i.e.*,  $\omega > 0$ . Next we assume that the nucleus has the shape of a uniaxial ellipsoid of radii  $a$ ,  $b$ , and  $b$ . Finally, we assume a homogeneous director field and, hence, we ignore the elastic free-energy cost for possible deformations of the director field. The generalization of classical nucleation theory to this case can be written as:

$$\Delta G = \int d^2S \gamma(1 + \omega(\mathbf{q} \cdot \mathbf{n})^2) - |\Delta\mu|\rho(4\pi/3)ab^2, \quad (5)$$

where the integral is over the surface of the ellipsoid. Introducing a Cartesian coordinate system  $(x, y, z)$  with the  $z$  axis along the long axis of the ellipsoid, such that the surface is described by  $z^2/a^2 + (x^2 + y^2)/b^2 = 1$ , we can parameterize the surface in terms of a polar and azimuthal angle  $\theta \in (0, \pi)$  and  $\phi \in (0, 2\pi)$ , respectively, as  $(x, y, z) = (b(\sin\theta)(\sin\phi), b(\sin\theta)(\cos\phi), a(\cos\theta))$ . Standard manipulations reveal a surface normal given

by  $\mathbf{q} = (a(\sin\theta)(\sin\phi), a(\sin\theta)(\cos\phi), b(\cos\theta))/\sqrt{a^2(\sin^2\theta) + b^2(\cos^2\theta)}$ , and a surface area element  $d^2S = b(\sin\theta)\sqrt{a^2(\sin^2\theta) + b^2(\cos^2\theta)}d\theta d\phi$ . If we now also assume that the nematic director field inside the droplet is uniform along the long axis such that  $\mathbf{n} = (0, 0, 1)$ , we find:

$$\mathbf{q} \cdot \mathbf{n} = \frac{b(\cos\theta)}{\sqrt{a^2(\sin^2\theta) + b^2(\cos^2\theta)}}. \quad (6)$$

Introducing the eccentricity parameter  $e = 1 - (b/a)^2$ , such that  $e = 0$  for spheres and  $e = 1$  for needle-shaped nuclei, we can write eqn (5) as:

$$\Delta G = 4\pi\gamma a^2 f(e, \omega) - |\Delta\mu|\rho(4\pi/3)a^3(1 - e), \quad (7)$$

with

$$f(e, \omega) = \sqrt{1 - e}(I_1(e) + \omega I_2(e))/2, \quad (8)$$

where

$$I_1(e) = \int_{-1}^1 d\xi \sqrt{1 - e\xi^2} = \sqrt{1 - e} + \frac{\arcsin\sqrt{e}}{\sqrt{e}} \quad (9)$$

$$I_2(e) = \frac{b^2}{a^2} \int_{-1}^1 d\xi \frac{\xi^2}{\sqrt{1 - e\xi^2}} \quad (10)$$

$$= (1 - e) \left( \frac{\arcsin\sqrt{e}}{e^{3/2}} - \frac{\sqrt{1 - e}}{e} \right).$$

Eqn (7)–(10) express the nucleation barrier in terms of the variational eccentricity  $e$ . For a given supersaturation and radius  $a$  of the droplet, the “equilibrium” eccentricity parameter  $e^*$  of the droplet minimizes  $\Delta G$  such that  $e^*$  is determined by:

$$\left. \frac{\partial \Delta G}{\partial e} \right|_{e^*} = 0, \quad (11)$$

which yields

$$\frac{2}{3}f(e^*, \omega) + (1 - e^*) \left. \frac{\partial f(e, \omega)}{\partial e} \right|_{e^*} = 0. \quad (12)$$

Interestingly, eqn (12) implies that  $e^*$  is a universal function of  $\omega$ , independent of *e.g.* the long radius  $a$ . This also implies that the aspect ratio of the critical nucleus  $a/b = 1/\sqrt{1 - e^*}$  is independent of supersaturation and cluster size. One also easily checks that eqn (12) gives  $e^* = 0$  if  $\omega = 0$ , *i.e.* an isotropic surface tension gives rise to a spherical droplet, as expected. For a given supersaturation  $\Delta\mu$ , the critical long axis  $a_{\text{crit}}$  of the critical nucleus satisfies  $\partial \Delta G / \partial a|_{a_{\text{crit}}} = 0$ , which yields

$$a_{\text{crit}} = \frac{2\gamma}{\rho|\Delta\mu|} \frac{f(e^*)}{1 - e^*} \equiv \frac{2\gamma}{\rho|\Delta\mu|} A(\omega), \quad (13)$$

where we defined the scaling function  $A(\omega)$  in terms of the equilibrium eccentricity  $e^*$  that satisfies eqn 12. Inserting  $a_{\text{crit}}$  into eqn (11) one obtains for the nucleation barrier

$$\Delta G_{\text{crit}} = \frac{16\pi}{3} \frac{\gamma^3}{(\rho\Delta\mu)^2} \frac{f^3(e^*)}{(1 - e^*)^2} \equiv \frac{16\pi}{3} \frac{\gamma^3}{(\rho\Delta\mu)^2} g(\omega), \quad (14)$$

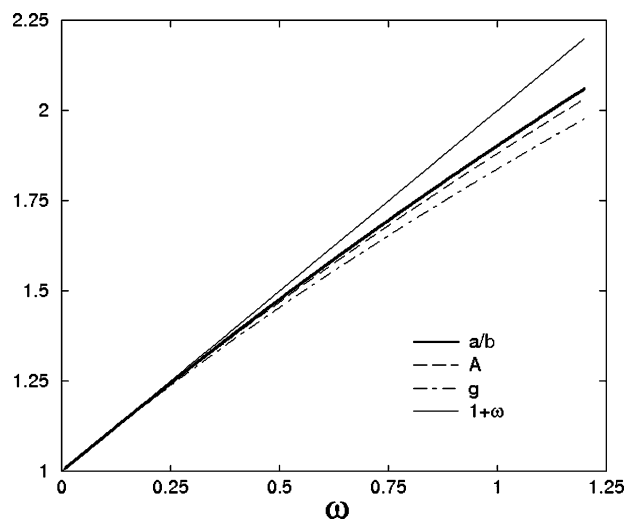


**Fig. 3** The aspect ratio  $a/b$  and the scaling functions  $A(\omega)$  and  $g(\omega)$  (see text) as a function of the anisotropy parameter  $\omega$  of the surface tension. For comparison, we also plot the initial slope for  $\omega \rightarrow 0$  given by  $1 + \omega$ .

which defines the scaling function  $g(\omega)$ . The  $\omega$ -dependence of  $a/b$ ,  $A(\omega)$ , and  $g(\omega)$  is shown in Fig. 3 for the  $\omega$ -regime of interest here. All three functions reduce, in the limit  $\omega \rightarrow 0$ , to  $1 + \omega + \mathcal{O}(\omega^2)$ . Note that for  $\omega = 0$  all three functions are unity, such that our expression for the critical radius  $a_{\text{crit}}$  and the nucleation barrier  $\Delta G_{\text{crit}}$  reduce to the standard CNT expressions for spherical droplets.

## IV. Results and discussion

### A. Hard-rod fluids

We present simulation results on the I–N transition in fluids of hard spherocylinders (HSC fluid). Some of the results presented here have already been published elsewhere.<sup>28</sup> We compress a well-equilibrated isotropic phase to a pressure beyond coexistence and we monitor different order parameters during the transformation. We first compress an isotropic fluid of  $N = 8640$  particles with  $L^* = 5$  at  $P^* = 1.27$  using MC simulations in the isobaric–isothermal ensemble. At this pressure, we find that the isotropic phase transforms spontaneously into a nematic phase. Upon compressing the isotropic phase, the density of the system increases gradually and we are not able to find a state on the metastable isotropic fluid branch. We find that phase separation sets in immediately after compressing as many small nematic clusters are formed throughout the system according to our cluster criterion (Fig. 4a). These clusters grow until they coalesce to form an interconnected ‘labyrinth’ structure (Fig. 4b). The nematic order parameter of this interconnected structure is small as the orientations of the original clusters of this labyrinth structure are very different. Subsequently, the nematic order parameter of the labyrinth structure increases as the clusters reorient. The immediate phase separation and the formation of a labyrinth structure is typical for spinodal decomposition, as has also been reported experimentally.<sup>19,20</sup> At this supersaturation, the isotropic phase is unstable. At lower supersaturations, one might expect to find the nucleation and growth regime. However, we were unable to find any metastable isotropic fluid phase or

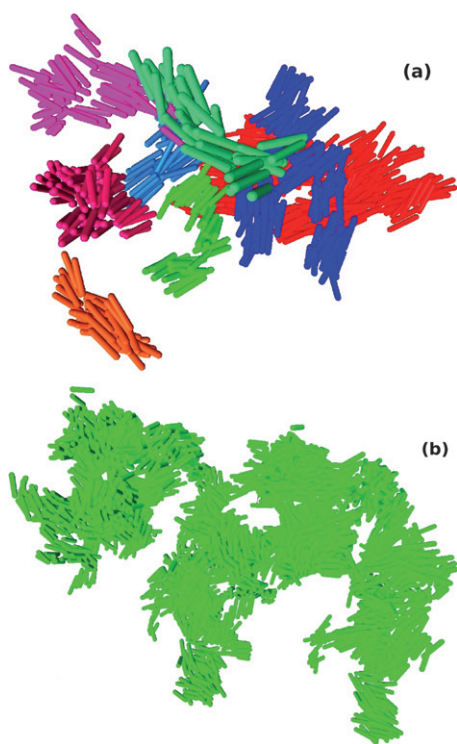


**Fig. 4** Typical intermediate configurations in the I–N transformation of a HSC fluid with  $L^* = 5$  at  $P^* = 1.27$ . (a) Configuration at the initial stage of the transition. Many small clusters are formed simultaneously with number of particles  $n = 462$  (red), 115 (blue), 69 (pink), 60 (light pink), 49 (light blue), 40 (orange), 34 (green) and 32 (light green). (b) In a later stage of the transition, these clusters coalesce and form an interconnected ‘labyrinth structure’.

nucleation and growth phenomenon for  $L^* = 5$ . This might be explained by the weak first-order character of the transition and the short metastable isotropic fluid branch.<sup>31</sup>

We also study the I–N transformation for a HSC fluid with  $L^* = 15$ . Here the I–N transition is strongly first order.<sup>31</sup> We first compress the isotropic fluid phase of  $N = 4320$  particles beyond coexistence to  $P^* = 0.125$ . At this supersaturation, the isotropic phase is unstable and we observe spontaneous formation of the nematic phase. We again find all the characteristics of spinodal decomposition. Fig. 5a shows the size of the biggest cluster in the system identified by our cluster criterion, the nematic order parameter of this cluster, and the global nematic order parameter as a function of the number of MC cycles. In the initial stage of phase separation, we find that many small nematic clusters appear throughout the system with a high nematic order. After about  $1 \times 10^5$  MC cycles, the nematic clusters coalesce and form an interconnected cluster: the nematic order parameter of this cluster drops suddenly as the original clusters have different orientations. Subsequently, the size and the nematic order of this interconnected cluster grow gradually until the whole system is transformed into the nematic phase. The observed phase-separation process has all the typical features of spinodal decomposition and is similar to the behavior described for  $L^* = 5$ .

Next we compress the system of  $L^* = 15$  at a lower supersaturated pressure of  $P^* = 0.105$ . We again observe that the isotropic phase transforms spontaneously into the nematic phase.

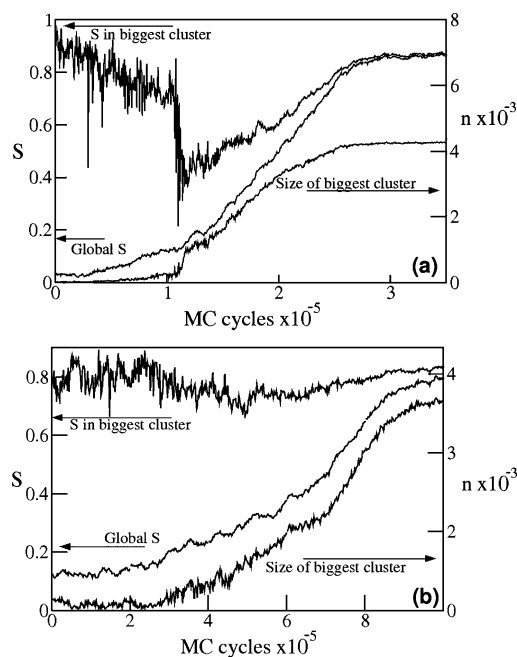


**Fig. 5** Evolution of the size of the biggest cluster  $n$  in the system (scale at right), the nematic order parameter  $S$  of the biggest cluster and of the total system (scale at left), for a HSC fluid with  $L^* = 15$  at (a)  $P^* = 0.125$  in the spinodal decomposition regime, and (b)  $P^* = 0.105$  in the nucleation and growth regime.

However, at this pressure, we observe all the characteristics of nucleation and growth. Upon compressing the system, we find that the system remains for a very long time in a metastable isotropic fluid phase at a density  $\rho^* = \rho\sigma^3 = 0.0147$ , slightly above the coexisting density of the isotropic fluid phase  $\rho_I^* = 0.0144$ . During the simulation, small nematic clusters are formed but they also disappear. After a certain number of MC cycles, a single nematic cluster starts to grow. Fig. 5b shows that the size of this single cluster grows gradually and that the nematic order of this cluster remains nearly constant. It is evident from Fig. 5b that the global nematic order parameter follows the growth of the nematic cluster. The long period that the system stays in a metastable isotropic fluid phase and the induction time before a single cluster starts to grow is typical for nucleation and growth. Unfortunately, we are not able to analyze the shape, size, and the structure of these nuclei, as the clusters dissolve or grow very quickly.

In summary, we find two different regimes in the I–N transition depending on the supersaturation. At high supersaturations we observe spinodal decomposition, while at low supersaturations we find nucleation and growth. At sufficiently low supersaturation  $P^* < 0.105$ , spontaneous nucleation never occurred on the timescales of our simulations. However, at these supersaturations we employ umbrella-sampling techniques<sup>2–4</sup> to study the free-energy barrier for nucleation and the structure of the nuclei. In the top panel of Fig. 6 we show the Gibbs free-energy barrier for  $P^* = 0.101, 0.102,$  and  $0.103$ . The top of the barrier determines the Gibbs free-energy of the critical cluster  $\Delta G_{\text{crit}}$  and its critical size  $n_{\text{crit}}$ . For  $P^* = 0.101$  clusters with  $n > 145$  start to percolate and it is therefore impossible to calculate the barrier height and the critical nucleus size. We note that the calculation of this Gibbs free-energy curve took more than 4 months of CPU

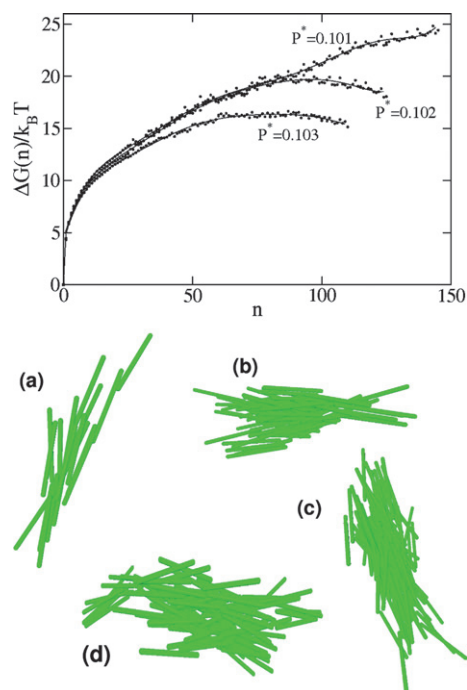


**Fig. 6** Top panel: Gibbs free energy of a HSC fluid with  $L^* = 15$  as a function of the nematic cluster size  $n$  at pressures  $P^* = 0.101, 0.102$ , and  $0.103$ . As a guide to the eye we have fitted the barrier with an 8th degree polynomial. Bottom panel: typical configurations of clusters with (a)  $n = 20$  particles, (b)  $n = 70$ , (c)  $n = 95$  and, (d)  $n = 120$  at  $P^* = 0.102$ .

time on a desktop PC. We can conclude that for this pressure, the height of the barrier is  $\beta\Delta G_{\text{crit}} > 25$  and  $n_{\text{crit}} > 145$ . For  $P^* = 0.102$ , we find  $\beta\Delta G_{\text{crit}} \approx 19.5$  with  $n_{\text{crit}} \approx 95$ , while for  $P^* = 0.103$ ,  $\beta\Delta G_{\text{crit}} \approx 16.0$  with  $n_{\text{crit}} \approx 83$ . Typical configurations of the clusters are shown in the bottom panel of Fig. 6.

We also employ the umbrella-sampling technique to study the shape and structure of the cluster as a function of its size. In Fig. 7, we show contour plots of the density profiles of the nematic particles in the cluster  $\rho^*(z, r)$ , and contour plots of the nematic order parameter profiles  $S(z, r)$  of all particles (isotropic and nematic), as a function of the distance from the center-of-mass of the cluster in the direction parallel ( $z$ ) and perpendicular ( $r$ ) to the nematic director. We show profiles for subcritical ( $n = 20$  and  $n = 80$ ), critical ( $n = 95$ ) and postcritical clusters ( $n = 120$ ). Fig. 7 shows that there is no qualitative difference between subcritical, critical, and postcritical clusters. All density profiles show that the shape of the nematic cluster is ellipsoidal with the long axis in the direction of the nematic director. The size of these clusters grows with the number of particles inside the cluster. We observe large fluctuations in the shape of the instantaneous clusters, and hence, the aspect ratio of the clusters varies in the range  $z_{\text{max}}/r_{\text{max}} \in [1.3, 2]$ . Inside the nematic clusters, the density profiles of the nematic particles also show an ellipsoidal symmetry, with a density decreasing gradually from the center to the surface of the cluster. Similarly, we also find ellipsoidal symmetric density profiles for the isotropic-like particles, *i.e.*, particles with an isotropic environment (not shown here).

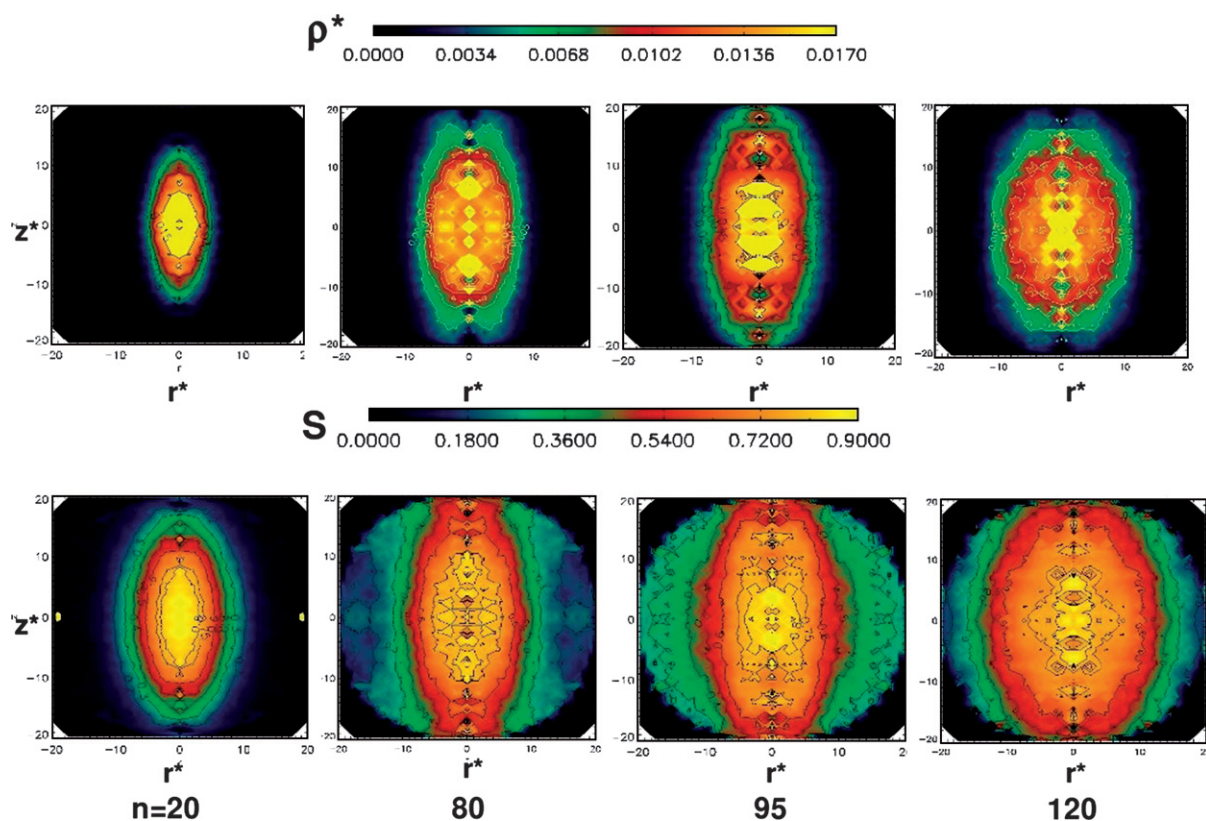


**Fig. 7** Contour plots for the density profiles (top row) and nematic order parameter profiles (bottom row) as a function of the distance from the center-of-mass of the cluster in the direction parallel ( $z^* = z/\sigma$ ) and perpendicular ( $r^* = r/\sigma$ ) to the nematic director for subcritical clusters ( $n = 20$  and  $80$ ), a critical cluster ( $n = 95$ ) and a postcritical cluster ( $n = 120$ ) at  $P^* = 0.102$  in a HSC fluid with  $L^* = 15$ .

However, in this case, the density in the center of the cluster is close to zero, and increases gradually from the center to the surface of the cluster. If we consider all particles, the total density at the cluster center has a value close to that of the corresponding bulk nematic phase, and the density decreases slightly further away from the cluster center. Far outside the nematic cluster, the density has a value close to that of the bulk isotropic phase at the corresponding pressure. We note that the density difference between the isotropic and nematic is very small. Hence, the density differs only slightly in and outside the nematic cluster.

In the bottom panel of Fig. 7, we present contour plots of the nematic order parameter profiles  $S(z, r)$  of all particles. The contour plots of the nematic order parameter profiles show a similar behavior as that of the density profiles, *i.e.*, an ellipsoidal symmetry around the center of the cluster with a nematic order parameter value decaying slowly from the center to the surface of the cluster. The value of the nematic order parameter at the center of the cluster is  $S \approx 0.8$ , which is consistent with the nematic order parameter of the corresponding bulk nematic phase. Note that the nematic order parameter is still relatively high outside the nematic cluster. The cluster is surrounded by a diffuse interface with a width of about the length  $L$  of the rods in contrast to a sharp step-like interface as assumed in CNT. The value of the interfacial width agrees well with previous simulation and theoretical studies on the isotropic–nematic planar interface.<sup>39–44</sup> It is worth mentioning that a looser cluster criterion, *i.e.*, lower values for the threshold values  $K_1$  and  $K_2$ , would detect the diffuse nematic layer, yielding larger sizes for the clusters. The similarities of the shape, aspect ratio, and ellipsoidal symmetry of  $S(z, r)$  and  $\rho^*(z, r)$  suggest a homogeneous nematic director field inside the cluster, which is not deformed near the surface of the cluster.

Finally, we compare the above simulation results for the HSC fluid with  $L^* = 15$  with the predictions obtained from the generalized classical nucleation theory as described in Section III. We first note that the present theory is based on the two assumptions that i) the clusters have an uniaxial ellipsoidal shape, and ii) the nematic director field is homogeneous such that elastic free-energy contributions due to deformations of the director field can be ignored. Our simulations are indeed in good agreement with these assumptions, thereby justifying the Gibbs free-energy expression in eqn (11) *a posteriori*. Minimizing this Gibbs free energy with respect to the eccentricity of the cluster, we found that  $alb$  is a universal function of  $\omega$ , independent of cluster size and supersaturation. In the limit  $\omega \rightarrow 0$ , the aspect ratio obeys  $alb \approx 1 + \omega$ . Using  $\gamma \approx 0.161k_B T/LD$  and  $\omega \approx 0.65$ , as predicted by Onsager theory for the planar isotropic–nematic interface,<sup>39,44,45</sup> and inserting these numbers into eqn (12), we find  $alb \approx 1.61$ . This value should be compared with our simulation result that  $alb = z_{\max}/r_{\max} \in [1.3, 2]$ , *i.e.* the theory is consistent with the simulation result. Similar results were obtained recently in a theoretical study based on a minimization of the free energy of a macroscopic nematic droplet.<sup>46,47</sup> Because of a competition between the interfacial tension, the anchoring strength, and bulk elasticity, this theory predicts different morphologies of nematic tactoids as a function of a dimensionless elastic stiffness  $\kappa \equiv K/\gamma V^{1/3}$  and  $\omega$ , where  $K$  denotes the Frank elastic constant, and  $V$  the volume of the droplet. Using again  $K$  and  $\omega$  from Onsager theory,<sup>39,44,45,48</sup> we find  $\kappa \gg 1$  with  $V$  equal to the size of our clusters. For these values, the theory predicts

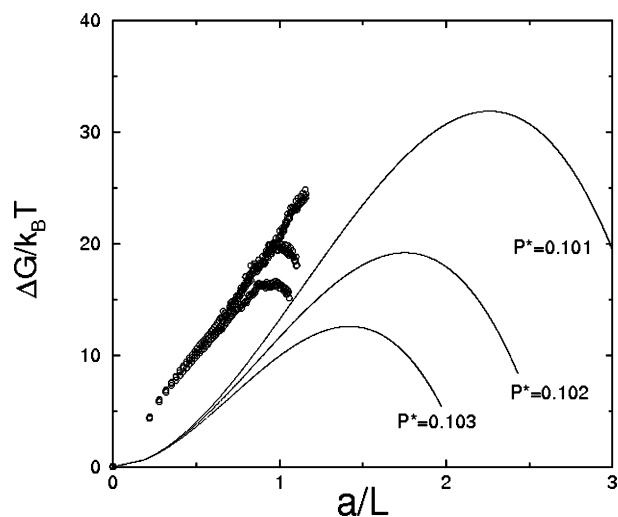


**Fig. 8** Gibbs free-energy  $\Delta G/k_B T$  as a function of the long semi-axis  $a$  of the cluster in units of the length  $L$  of the spherocylinder as obtained by theory (solid line) and by simulation (symbols) for a HSC fluid with  $L^* = 15$  at  $P^* = 0.100, 0.101$ , and  $0.102$ .

homogeneous spheroidal (ellipsoidal) droplets with an aspect ratio of  $1 + \omega \approx 1.65$ . Our simulation results are in good agreement with these theoretical predictions.

In addition, we calculate the theoretical Gibbs free-energy barrier as a function of the long semi-axis  $a$  of the cluster. In Fig. 8, we compare the theoretical predictions for the Gibbs free-energy barrier with our simulation results. We find that the theoretical predictions for both the long semi-axis as well as the barrier height are of the same order as those obtained in the simulations. However,  $a$  is underestimated systematically in the simulations compared to CNT, which is probably due to the strict cluster criterion that we had to use in our umbrella sampling in order to be able to distinguish the nematic clusters from the isotropic phase. Above, we already mentioned that a more detailed investigation of the structure of the nematic clusters in our simulations shows that the clusters are surrounded by a diffuse nematic layer with a width of about the length  $L$  of the rods. A simple way to take into account the diffuse interface is by simply adding about half the interfacial width ( $\approx 0.5L$ ) to the long semi-axis  $a$ , *i.e.*, the free-energy barriers for nucleation are shifted in horizontal direction by about 0.5 in Fig. 8. Employing this horizontal shift of the free-energy barriers, we now find reasonable agreement between theory and simulations. Finally, we note that a more accurate value for the surface tension  $\gamma$  has been obtained recently by simulations of a HSC fluid with  $L^* = 15$ .<sup>49</sup> We check that the theoretical predictions did not change considerably by using this value for  $\gamma$ . For consistency, we use the values from Onsager theory for  $\omega$ ,  $\gamma$ , and  $K$  in our calculations. In conclusion, our simulations agree qualitatively with the theoretical prediction of our generalization of CNT to anisotropic particles, where we assume a homogeneous director field and clusters of ellipsoidal shape.

## B. Binary mixture of hard rods and polymers

We now focus on the I–N transition in a binary mixture of colloidal hard rods and non-adsorbing polymer. The addition

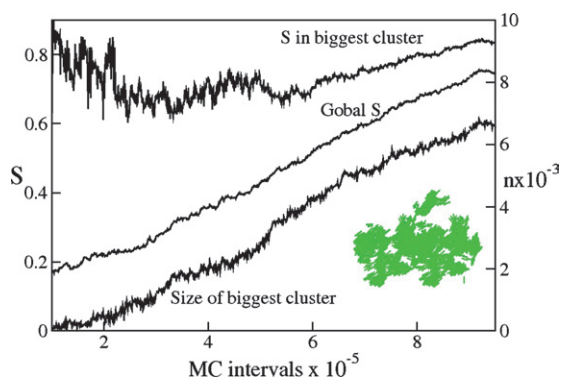


**Fig. 9** Evolution of the size of the biggest cluster  $n$  in the system (scale at right), the nematic order parameter  $S$  of the biggest cluster and of the total system (scale at left) for a mixture of rods and polymers represented by an effective pair potential with  $L^* = 5$ , radius of gyration of the polymer  $R_g = 0.25\sigma$ , and polymer fugacity  $z_p = 0.514$  at  $P^* = 1.2$ . The inset shows a typical configuration of the labyrinth structure observed in the spinodal decomposition regime.

of polymer to a suspension of rods, induces an effective polymer-mediated attraction between the rods, which we model by an effective pair potential.<sup>29</sup> This pair potential depends on the relative orientation of the rods and the center-of-mass distance vector. Surprisingly, our results on the I–N nucleation is hardly affected by the attractive interactions.

We study the I–N transition for a system of hard spherocylinders with  $L^* = 5$ , polymer fugacity  $z_p = 0.514$ , and polymer radius of gyration  $R_g = 0.25\sigma$ . First, we quench a well-equilibrated isotropic configuration to a pressure beyond bulk coexistence. In Fig. 9, we show the evolution of the size of the biggest cluster  $n$  in the system, the nematic order parameter  $S$  of the biggest cluster, and of the total system for a relatively large supersaturation of  $P^* = 1.20$ . We find an I–N transformation that is similar to the spinodal decomposition case that we also found in the largely supersaturated hard-rod fluids: In the early stage of the transition, many clusters appear simultaneously. These clusters start to coalesce and form an interconnected ‘labyrinth’ structure. As the original clusters have different orientations, the system-spanning interconnected cluster has a lower nematic order parameter than the original ones. The inset of Fig. 9 shows a typical configuration of the percolating interconnected cluster. Subsequently, the nematic order of this cluster increases as the original clusters reorient. At the same time, the size of the cluster grows by addition of new particles to the cluster, until the whole system is transformed into the nematic phase.

At lower supersaturation, we were unable to find a spontaneous transition from the isotropic to the nematic phase within the time of our simulations. In this regime, we use again umbrella-sampling techniques to study the free-energy barrier for nucleation and the structure of the nuclei. In Fig. 10, we show the Gibbs free-energy barrier for a rod–polymer mixture at supersaturations  $P^* = 0.90$  and  $0.91$ . At the lowest supersaturation of these,  $P^* = 0.90$ , we are not able to find the maximum of the barrier as the biggest nematic cluster starts to percolate. We can only conclude here that the height of the barrier is  $\Delta G_{\text{crit}} > 25k_B T$  and  $n_{\text{crit}} > 250$  for  $P^* = 0.90$ . For  $P^* = 0.91$ , we find  $\Delta G_{\text{crit}} \approx 14k_B T$  and  $n_{\text{crit}} \approx 110$ .

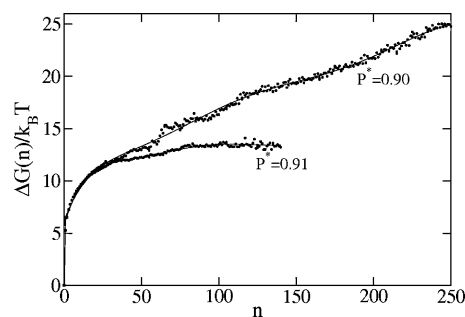


**Fig. 10** Gibbs free energy  $\Delta G/k_B T$  as a function of the nematic cluster size  $n$  of a rod–polymer mixture represented by an effective pair potential for the rods with  $L^* = 5$ , radius of gyration  $R_g = 0.25\sigma$ , and polymer fugacity  $z_p = 0.514$  at pressure  $P^* = 0.90$  and  $0.91$ . As a guide to the eye we have fitted the barrier with an 8th degree polynomial.

For  $P^* = 0.91$ , we analyze the structure of the clusters for different cluster sizes. Contour plots of the density and nematic order parameter profiles are shown in Fig. 11. In the top panel of Fig. 11, we present contour plots of the density profiles of the nematic particles in the cluster  $\rho^*(z, r)$  for cluster sizes:  $n = 60$  and  $n = 90$  (subcritical),  $n = 110$  (critical), and  $n = 130$  (postcritical). In the bottom panel, we show contour plots of the nematic order parameter profiles  $S(z, r)$  of all the particles for the same cluster sizes as displayed for the density profiles. Again, we find that all density profiles of the nematic particles in the cluster are ellipsoidal in symmetry, as also found for the HSC fluids. However, the shape of the clusters seems to be more rectangular for the rod–polymer mixtures. The density at the center of the cluster is higher than far away from the cluster and has a value close to that of the corresponding bulk nematic phase. The aspect ratio of the clusters vary in the range  $z_{\text{max}}/r_{\text{max}} \in [1.3, 1.8]$ . As in the case of the HSC fluid, we again observe significant fluctuations in the aspect ratio of the instantaneous clusters. The contour plots of the nematic order parameter profiles present a similar behavior, an ellipsoidal symmetry with values close to the corresponding nematic bulk phase in the center of the nucleus and a value close to the isotropic phase far away from the center of the cluster. The similarities of the shape, aspect ratio, and symmetry of  $S(z, r)$  and  $\rho^*(z, r)$  suggest again a homogeneous director field in the cluster, without significant director distortions and anchoring to the cluster surface.

Fig. 11 shows clearly that there are no qualitative difference between subcritical, critical, and postcritical clusters, as was also found for the HSC fluid with  $L^* = 15$ . We conclude, that the shape, aspect ratio, symmetry, and director field are independent of cluster size for the systems and conditions considered here.

## V. Summary and conclusions

In this paper, we have used computer simulations to study the isotropic–nematic transformation for two different types of systems of rods: i) fluids of colloidal hard rods of lengths  $L^* = 5$  and  $15$ , and ii) a binary mixture of hard rods with non-absorbing polymer represented by an effective one-component system of attracting rods. In our study we have found, for both type of systems, two regimes depending on the supersaturation. At high supersaturation of the isotropic phase, the transition to the

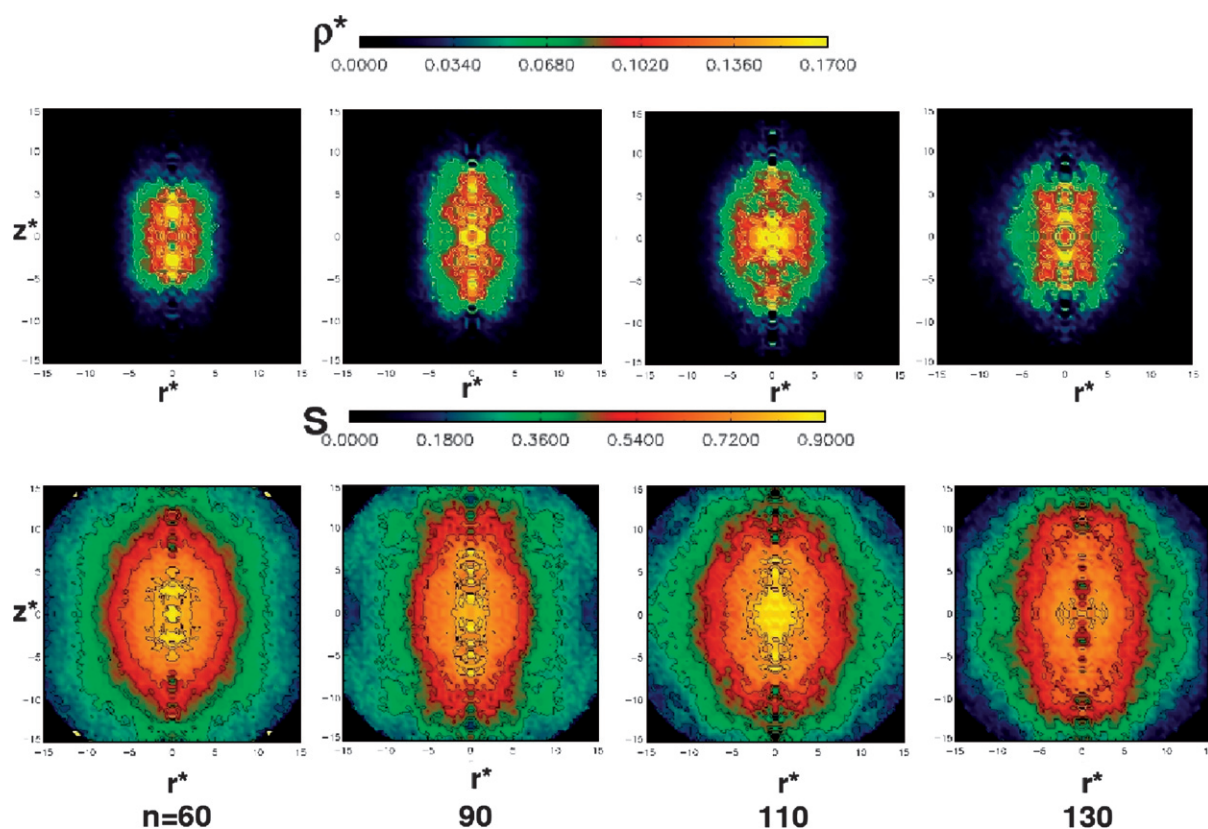


**Fig. 11** Contour plots of the density profiles (top row) and nematic order parameter profiles (bottom row) as a function of the distance from the center-of-mass of the cluster in the direction parallel ( $z^* = z/\sigma$ ) and perpendicular ( $r^* = r/\sigma$ ) to the nematic director for a cluster size  $n = 60$  and  $n = 90$  (subcritical),  $n = 110$  (critical), and  $n = 130$  (postcritical) at  $P^* = 0.91$  in a mixture of rods with  $L^* = 5$  and polymers with radius of gyration  $R_g = 0.25\sigma$ , and at polymer fugacity  $z_p = 0.514$ .

nematic phase occurs due to the formation of many small nematic clusters. These droplets coalesce and form an irregular and ‘labyrinth’ structure that grows until the whole system is transformed into the nematic phase. This type of coarsening strongly resembles that of spinodal decomposition. The existence of spinodal decomposition has been predicted theoretically by Onsager,<sup>37</sup> and has been studied experimentally in Ref. 19. In Ref. 27, the IN spinodals for pure hard rods were pinpointed by a vanishing collective rotational diffusion coefficient. For attractive rods, spinodal demixing is probably governed by rotational and translational diffusion. It would therefore be interesting to investigate the spinodal decomposition kinetics using our effective polymer-mediated attractive rod–rod interactions in Brownian dynamics simulations.

At lower supersaturation the mechanism is different: first, the system stays for a long period of time in the metastable isotropic fluid state. After a certain induction time, a single cluster starts to grow until the whole system is transformed into the nematic phase. These characteristics are typical for nucleation and growth. When the transition is due to nucleation and growth, the system has to overcome a Gibbs free-energy barrier. The structure of the nuclei observed in the nucleation and growth regime are very similar for both the hard-rod fluids and the rod–polymer mixture, at least for the parameters studied here. They both show nuclei with an ellipsoidal shape with an aspect ratio  $1.3 < a/b < 2$ , and a uniform nematic director field inside the cluster.

Our results are in accordance with experimental observations of both phenomena in solutions of boehmite rods,<sup>19</sup> F-actin,<sup>24</sup> clay rods,<sup>23</sup> and on mixtures of rod-like viruses and polymer.<sup>18,22</sup> Our simulations show, however, that the critical cluster size is many times smaller than the experimentally observed tactoids. This suggests that the ‘long-lived and stable’ tactoids that are observed experimentally are post-critical and are in a late stage of the phase separation, *i.e.*, the tactoidal growth regime. We hope that our findings stimulate new experiments on the nucleation process at an early stage of the phase separation.

We have also discussed our results in the light of classical nucleation theory (CNT). We modified the standard CNT to non-spherical nuclei and anisotropic surface tensions. We assume a homogeneous nematic director field, thereby ignoring the free-energy cost for elastic deformations. We also assume an ellipsoidal shape for the nuclei. We find that our simulation results agree qualitatively with the predictions obtained from the generalized CNT. The aspect ratio of the nuclei and the barrier height are reasonably well predicted. In order to compare the size of the critical cluster, we have to realize that our cluster criterion is very strict and that the simulated clusters are surrounded by a diffuse interface with an interfacial width of the order of the length of the rods. Simply adding half the interfacial width to the semi-axis of the droplets gives, however, reasonable agreement between the free-energy barriers as obtained from simulations and theory. It is worth noting that the long semi-axis

of the critical droplets is of the same order of magnitude as the interfacial width, *i.e.* critical nucleus is actually not at all a bulk nematic state. We therefore feel that there is an urgent need to improve the CNT of these systems by taking into account the diffuse character of the interface, *i.e.*, to allow for an inhomogeneous density profile inside the clusters.

Finally, we note that our new cluster criterion opens up a whole new field in which the kinetics of many other phase transitions of anisotropic particles can be studied, including transitions in molecular fluids and in systems of attractive rods, for which recent experiments show intriguing phenomena such as surface-induced smectic phases on nematic tactoids, smectic membranes winding off from tactoids as twisted ribbons, and melting of lamellar phases.<sup>18,50</sup> The study of the isotropic–smectic transition of short hard rods is in progress and will be reported elsewhere. In future work, we plan to investigate the isotropic-to-smectic transition in mixtures of hard rods and polymers at higher polymer concentrations, using the simulation techniques presented here. We hope that our study will shed light on the transient structures found experimentally.<sup>18</sup>

## VI. Acknowledgements

We thank E. Sanz and M. Bier for useful discussions. We kindly acknowledge S. Savenko for his help with the effective polymer-mediated pair potential (the “Slava” potential), and for providing us with data on the equation of state. NWO-CW is acknowledged for the TOP-CW funding.

## VII. References

- 1 K. F. Kelton, *Solid State Phys.*, 1991, **45**, 75.
- 2 G. M. Torrie and J. P. Valleau, *Chem. Phys. Lett.*, 1974, **28**, 578.
- 3 C. H. Bennet, in *Algorithms for Chemical Computations*, ed. R. E. Christofferson, American Chemical Society, Washington, DC, 1977.
- 4 D. Chandler, *J. Chem. Phys.*, 1978, **68**, 2959.
- 5 D. Moroni, P. R. ten Wolde and P. G. Bolhuis, *Phys. Rev. Lett.*, 2005, **94**, 235703.
- 6 P. G. Bolhuis, D. Chandler, C. Dellago and P. L. Geissler, *Annu. Rev. Phys. Chem.*, 2002, **53**, 291.
- 7 C. Dellago, P. G. Bolhuis and P. L. Geissler, *Adv. Chem. Phys.*, 2002, **123**, 1.
- 8 R. J. Allen, P. B. Warren and P. R. ten Wolde, *Phys. Rev. Lett.*, 2005, **94**, 018104.
- 9 C. Valeriani, E. Sanz and D. Frenkel, *J. Chem. Phys.*, 2005, **122**, 194501.
- 10 R. J. Allen, D. Frenkel and P. R. ten Wolde, *J. Chem. Phys.*, 2006, **124**, 024102.
- 11 P. R. ten Wolde, M. J. Ruiz-Montero and D. Frenkel, *Phys. Rev. Lett.*, 1995, **75**, 2741.
- 12 P. R. ten Wolde, M. J. Ruiz-Montero and D. Frenkel, *J. Chem. Phys.*, 1996, **104**, 9932.
- 13 E. Sanz, C. Valeriani, D. Frenkel and M. Dijkstra, *Phys. Rev. Lett.*, 2007, **99**, 055501.
- 14 S. Alexander and J. McTague, *Phys. Rev. Lett.*, 1978, **41**, 702.
- 15 Y. C. Shen and D. W. Oxtoby, *Phys. Rev. Lett.*, 1996, **77**, 3585.
- 16 D. W. Oxtoby and R. Evans, *J. Chem. Phys.*, 1988, **89**, 7521.
- 17 D. W. Oxtoby, *Acc. Chem. Res.*, 1998, **31**, 91.
- 18 Z. Dogic and S. Fraden, *Philos. Trans. R. Soc. London, Ser. A*, 2001, **359**, 997.
- 19 M. P. B. van Bruggen, J. K. G. Dhont and H. N. W. Lekkerkerker, *Macromolecules*, 1999, **32**, 2256.
- 20 P. Oakes, J. Viamontes and J. X. Tang, *Phys. Rev. E: Stat., Nonlinear, Soft Matter Phys.*, 2007, **75**, 061902.
- 21 M. P. Lettinga, K. Kang, P. Holmqvist, A. Imhof, D. Derks and J. K. G. Dhont, *Phys. Rev. E: Stat., Nonlinear, Soft Matter Phys.*, 2006, **73**, 011412.
- 22 M. P. Lettinga et al., *J. Phys.: Condens. Matter*, 2005, **17**, S3609.
- 23 Z. X. Zhang and J. S. van Duijneveldt, *J. Chem. Phys.*, 2006, **124**, 154910.
- 24 J. Viamontes, P. Oakes and J. X. Tang, *Phys. Rev. Lett.*, 2006, **97**, 118103.
- 25 T. Schilling and D. Frenkel, *Phys. Rev. Lett.*, 2004, **92**, 085505.
- 26 T. Schilling and D. Frenkel, *Comput. Phys. Commun.*, 2005, **169**, 117.
- 27 Y.-G. Tao, W. K. Otter, J. K. G. Dhont and W. J. Briels, *J. Chem. Phys.*, 2006, **124**, 134906.
- 28 A. Cuetos and M. Dijkstra, *Phys. Rev. Lett.*, 2007, **98**, 095701.
- 29 S. V. Savenko and M. Dijkstra, *J. Chem. Phys.*, 2006, **124**, 234902.
- 30 S. C. McGrother, D. C. Williamson and G. Jackson, *J. Chem. Phys.*, 1996, **104**, 6755.
- 31 P. Bolhuis and D. Frenkel, *J. Chem. Phys.*, 1997, **106**, 666.
- 32 P. R. ten Wolde and D. Frenkel, *J. Chem. Phys.*, 1998, **109**, 9901.
- 33 P. R. ten Wolde and D. Frenkel, *J. Chem. Phys.*, 1999, **110**, 1591.
- 34 V. K. Shen and P. G. Debenedetti, *J. Chem. Phys.*, 1999, **111**, 3581.
- 35 S. Auer and D. Frenkel, *Nature*, 2001, **409**, 1020.
- 36 G. J. Vroege and H. N. W. Lekkerkerker, *Rep. Prog. Phys.*, 1992, **55**, 1241.
- 37 L. Onsager, *Ann. N. Y. Acad. Sci.*, 1949, **51**, 627.
- 38 R. van Roij, *Eur. J. Phys.*, 2005, **26**, S57.
- 39 Z. Y. Chen and J. Noolandi, *Phys. Rev. A: At., Mol., Opt. Phys.*, 1992, **45**, 2389.
- 40 M. Dijkstra, R. van Roij and R. Evans, *Phys. Rev. E: Stat., Nonlinear, Soft Matter Phys.*, 2001, **63**, 051703.
- 41 R. van Roij, M. Dijkstra and R. Evans, *Europhys. Lett.*, 2000, **49**, 350.
- 42 R. van Roij, M. Dijkstra and R. Evans, *J. Chem. Phys.*, 2000, **113**, 7689.
- 43 S. Wolfsheimer, C. Tanase, K. Shundyak, R. van Roij and T. Schilling, *Phys. Rev. E: Stat., Nonlinear, Soft Matter Phys.*, 2006, **73**, 061703.
- 44 K. Shundyak and R. van Roij, *J. Phys.: Condens. Matter*, 2001, **13**, 4789; K. Shundyak and R. van Roij, *Phys. Rev. Lett.*, 2002, **88**, 205501; K. Shundyak and R. van Roij, *Phys. Rev. E: Stat., Nonlinear, Soft Matter Phys.*, 2003, **68**, 061703.
- 45 C. Tanase, unpublished.
- 46 P. Prinsen and P. van der Schoot, *Phys. Rev. E: Stat., Nonlinear, Soft Matter Phys.*, 2003, **68**, 021701.
- 47 P. Prinsen and P. van der Schoot, *Eur. Phys. J. E*, 2004, **13**, 35.
- 48 A. Poniewierki and J. Stecki, *Mol. Phys.*, 1979, **38**, 1931.
- 49 R. L. C. Vink, S. Wolfsheimer and T. Schilling, *J. Chem. Phys.*, 2005, **123**, 074901.
- 50 A. M. Alsayed, Z. Dogic and A. G. Yodh, *Phys. Rev. Lett.*, 2004, **93**, 057801.